Int J Adv Manuf Technol (2008) 37:1061–1068
DOI 10.1007/s00170-007-1057-1

ORIGINAL ARTICLE

Comparison between response surface methodology and radial basis function network for core-center drill in drilling composite materials

C. C. Tsao

Received: 29 January 2007 / Accepted: 18 April 2007 / Published online: 23 May 2007

Abstract Drilling using twist drill is the most frequently used secondary machining for fiber-reinforced composite laminates and delamination is the most important concern during drilling. The drill design and drilling parameters associated with thrust distribution on the drilling-induced delamination are presented. The core-center drill has been found to be more advantageous than the core drill in reference and practice experiences. Response surface methodology (RSM) is a very practical, economical, and useful tool for the modeling and analysis of experimental results using polynomials as local approximations to the true input/output relationship. Due to the radial basis function network's (RBFN) fast learning speed, simple structure, local tuning, and global generalization power, researchers in the field of manufacturing engineering have been using RBFN in nonlinear manufacturing studies. The present paper compares these two techniques using various drilling parameters (diameter ratio, feed rate, and spindle speed) to predict the thrust force for a core-center drill in drilling composite materials. The obtained results indicated that RBFN is a practical and an effective way for the evaluation of drilling-induced thrust force.

Keywords Core-center drill · Delamination · Radial basis function network (RBFN) · Response surface methodology (RSM) · Thrust force

C. C. Tsao (✉)
Department of Automation Engineering,
Tahua Institute of Technology,
Hsinchu 30740, Taiwan, Republic of China
e-mail: aetcc@msdb.thit.edu.tw

1 Introduction

Among all the material-removal processes, drilling using a twist drill is the most commonly applied method for drilling holes for riveting and fastening structural assemblies [1]. The importance of the drilling process is evident from the constant developments in drill design in search for improved drill performance and a more cost-effective production of drills and holes. It is well known that the geometry of the drill point has a significant effect on the performance of a twist drill [2, 3]. Using multifaceted drills, Wu reduced up to 70% of the thrust force compared to that of the conventional twist drill [4]. Doerr et al. designed a drill for cutting materials toward the hole center and for shearing at the hole edge [5]. Friedrich et al. cited the "split" or "crankshaft" point, which is very popular in the aircraft and automotive industries [6]. Haggerty and Ernst found that "spiral" point drills performed much better than conventional ones [7]. In the drilling process, some key parameters, e.g., feed rate and cutting speed, which govern the final quality of the composites, should also be considered [8–11]. A general overview of the various possibilities for composites machining can be found in [12].

Modern composites using fiber-reinforced matrices of various types have created a revolution in high-performance structure. Advanced composite materials offer significant advantages in strength and stiffness as well as being lightweight relative to conventional metallic materials. A major concern for drilling holes in composite materials is the delamination that occurs in the entrance as well as in the exit surface of the workpiece. The size of the delamination zone has been shown to be related to the thrust force developed during the drilling process and there exists a "critical thrust force" below which no damage occurs [8]. Some researchers show that the stacking sequence and ply

angle also affect the thrust force and delamination growth when drilling composite materials [13, 14]. Apart from those of the twist drill, the effects of various drill geometry were less discussed analytically except for our previous works [15–18]. Hocheng and Tsao developed a series of analytical models for various drills (saw drill, candle stick drill, core drill and step drill) for correlating the thrust force at the onset of delamination [15, 16]. Mathew et al. reported using the trepanning tool to reduce the thrust force and torque when drilling glass fiber-reinforced plastic (GFRP) laminates [17]. Piquet et al. showed the capabilities of the specific cutting tool in drilling thin carbon/epoxy plate [18]. In addition to the studies on the above-mentioned drills, the critical thrust force for a core-center drill at the onset of delamination is predicted and compared with that for a core drill and a twist drill.

Response surface methodology is a very practical, economical, and useful tool for the modeling and analysis of machining processes using polynomials as local approximations to the true input/output relationship [19–21]. The greatest advantage of an artificial neural network (ANN) is its ability to model complex nonlinear, multi-dimensional functional relationships without any prior assumptions about the nature of the relationships, and the network is built directly from experimental data by its self-organizing capabilities [22, 23]. Because a radial basis function network (RBFN) has many advantageous features such as fast learning speed, simple structure, local tuning and global generalization power, many researchers in the field of manufacturing engineering have been using RBFN in nonlinear manufacturing studies [24–26]. Jang and Sun showed that the functional behavior of an RBFN is actually equivalent to that of a fuzzy inference system (FIS) under minor restrictions [27]. The widely used algorithms of neural network in predictive modeling are the back propagation neural network (BPNN) and radial basis function network. BPNN have accomplished this task by learning from a series of data sets related to the system and then applying what was learned to approximate or predict the corresponding output. Mason et al. found that RBFN is more suitable than BPNN in solving system control problems [28]. RBFN not only has the same prediction capability as BPNN, but also offers the benefits of easier parameter design. Kim and Park applied both RBFN and statistical regression model to the plasma etch process to predict etch rate and surface roughness [29]. They discovered that RBFN could provide better prediction capability than statistical regression. A general overview of the various principles of the neural network approach for predicting certain properties of polymer composite materials was provided in [30]. The purpose of this study is to compare the RSM and RBFN techniques in the prediction of drilling-induced thrust force using various drilling parameters (diameter ratio, feed rate and spindle speed) for core-center drill in drilling carbon fiber-reinforced plastic (CFRP) laminates.

2 Response surface methodology (RSM)

Box and Draper first developed the RSM for the model fitting of physical experiments [31]. RSM uses statistical design of experimental technique and least-square fitting method in the model generation phase. The carefully designed experiments aim to obtain the relationship between the response (output variable) and various machining parameters (input variables), and to optimize or predict the response. The relationship between the response variable of interest and the input variables is usually not known. In general, a second-order polynomial response surface mathematical model is employed to analyze the parametric influences on various response criteria. The second-order model helps understand the second-order effect of each factor separately and the two-way interaction amongst these factors combined. This second-order mathematical model can be represented as follows:

$$Y = b_o + \sum_{i=1}^{n} b_i X_i + \sum_{i=1}^{n} b_{ii} X_{ii}^2 + \sum_{i<j} b_{ij} X_i X_j + \varepsilon \qquad (1)$$

where Y is the corresponding response, X_i is the input variables, X_{ii}^2 and X_iX_j are the squares and interaction terms of these input variables, b_o, b_i, b_{ij} and b_{ii} are the regression coefficients of parameters and ε is the experimental error.

3 Radial basis function network (RBFN)

The RBFN is constructed with input, output and hidden layers of Gaussian activation functions. The network is capable of performing nonlinear mapping of the input features onto the output. The structure of RBFN has only one hidden layer that applies a multidimensional nonlinear transformation from the input space to the hidden space. Gaussian function in the hidden layer is the most commonly used basis function for the RBFN. It has been established that an RBFN with sufficient number of Gaussian basis functions in the hidden layer can be used as a universal approximator [32]. A schematic diagram of RBFN is shown in Fig. 1. The output of the ith receptive field unit (or hidden unit) is

$$R_i(\vec{x}) = R_i\left(\frac{\left\|\vec{x} - \vec{C}_i\right\|}{\sigma_i}\right) i = 1, 2, \cdots, H \qquad (2)$$

where $\vec{x}$ is input vector, $\vec{C}_i$ is a centre vector, H is the number of receptive field units, and σ_i is the variance of the

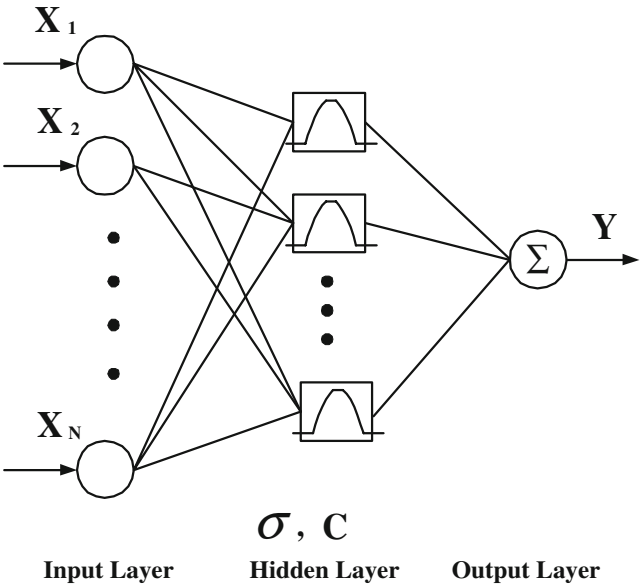

Fig. 1 A schematic diagram of radial basis function network

Gaussian function. The output is the weighted sum of the function value associated with each receptive field:

$$Y(\vec{x}) = \sum_{i=1}^{H} R_i W_i \tag{3}$$

where W_i is the connection weight of the output layer. The error function (E) is defined as:

$$E = \frac{1}{2}\sum_i (T_i - Y_i)^2 \tag{4}$$

where T_i is the desired output and Y_i is the actual output. For fast identification of parameters, the gradient-descent method was used. The parameters of RBFN can update as follow:

$$\Delta C_j = -\eta \frac{\partial E}{\partial C_j} + \alpha C_{old} \quad \eta, \alpha \in (0, 1] \tag{5}$$

$$\Delta \sigma_j = -\eta \frac{\partial E}{\partial \sigma_j} + \alpha \sigma_{old} \tag{6}$$

$$\Delta W_j = -\eta \frac{\partial E}{\partial W_j} \tag{7}$$

$$C_{new} = C_{old} + \Delta C_j \tag{8}$$

$$\sigma_{new} = \sigma_{old} + \Delta \sigma_j \tag{9}$$

$$W_{new} = W_{old} + \Delta W_j \tag{10}$$

where η is the learning rate and α is the momentum coefficient. In this study, the criterion of convergent error (root mean square error (RMSE)) can be expressed as

$$RMSE = \frac{1}{\|T_i - Y_i\|}\sqrt{\frac{1}{2}\sum_i (T_i - Y_i)^2} \tag{11}$$

4 Experimental procedure

4.1 Specimen preparation and drilling test

In the present experimental study, the composite materials for drilling were fabricated from the woven WFC200 fabric carbon fiber/epoxy matrix using autoclave molding. The stacking sequence and thickness of the CFRP laminates were $[0/90]_{12S}$ and approximately 6 mm, respectively. Specimens of size 60×60 mm were cut on a water-cooled diamond table saw. The fiber volume fraction is 0.55. The diameter of the core-center drill is 10 mm with one end of the tube coated with diamond grits and its length and thickness are 12 and 1 mm, respectively. The internal core-center is a twist drill as shown in Fig. 2. The point angle and helix angle of twist are 118° and 25°, respectively. The radii of the twist drill are 4.0 mm, 5.5 mm and 7.4 mm, respectively. Drilling tests were carried out on a LEADWELL MCV-610AP vertical machining center with 5.5 kW spindle power and three-axis FANUC controllers as shown in Fig. 3. The mean thrust forces at the exit of the drill bits during drilling were measured with a Kistler 9273 piezoelectric dynamometer. Meanwhile, the drilling and thrust forces signals were transmitted to Kistler 5011 charge amplifiers and stored in a TEAC DR-F1 digital recorder subsequently. The amplifier has to stabilize for at least an hour. All tests were run without coolant at spindle speeds of 800, 1,000, and 1,200 rpm and feed rates of 8, 12, and 16 mm/min, respectively.

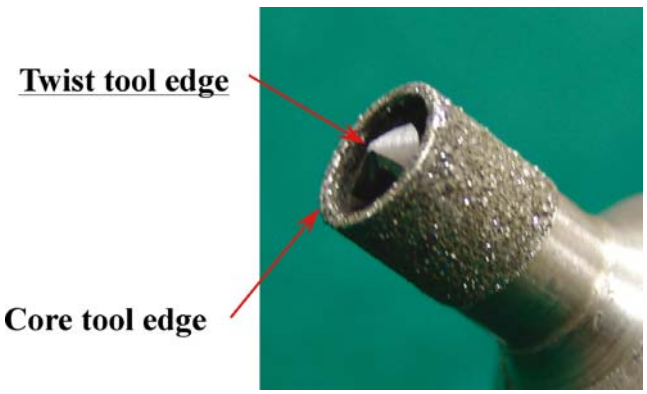

Fig. 2 Core-center drill

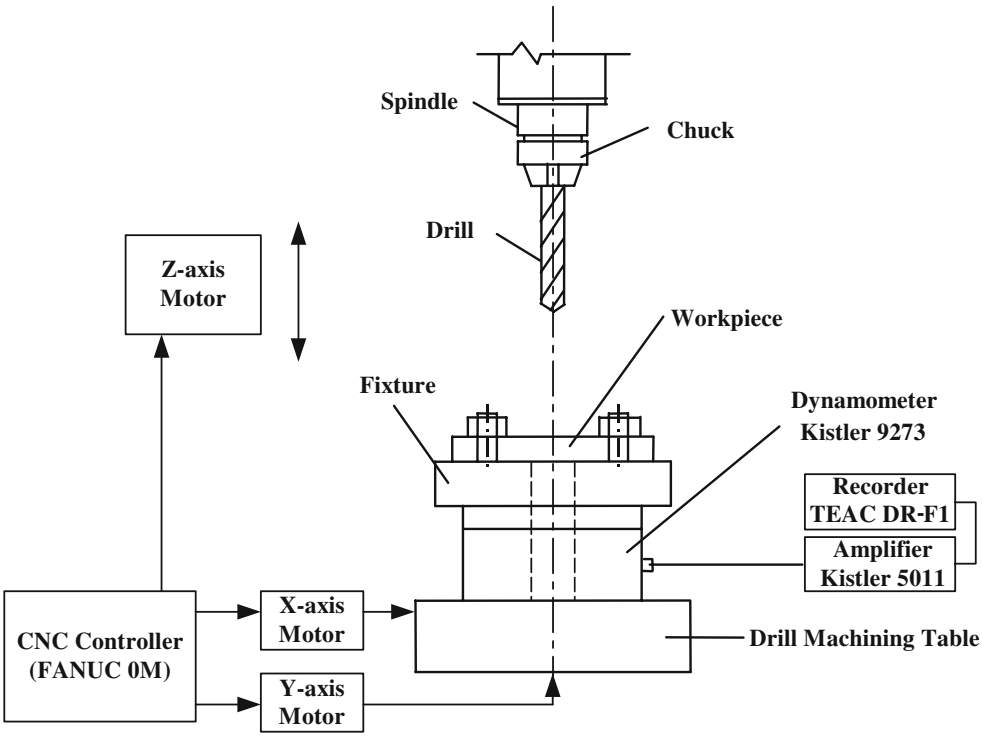

Fig. 3 Experimental setup to measure the thrust force

4.2 Measurement of peripheral core edge-induced thrust force (γ)

To estimate the portion of the peripheral core edge-induced thrust force, an experiment using a simple twist drill was designed with extreme care. The same specimen was used in all experiments for each cutting condition. The thrust force acting on the peripheral core edge for a specific cutting condition was estimated by subtracting the thrust force when drilling with a simple twist drill from that when drilling with a core-center drill.

5 Results and discussions

5.1 Analysis of response surface

Experimental results of the thrust force for drilling composite materials with core-center drill are shown in Table 1. The mathematical relationship for correlating the thrust force (F) and the considered drilling variables (diameter ratio (d), feed rate (f) and spindle speed (N)) is obtained from the coefficients resulting using the SPSS software as follows:

$$F = -57.441 - 3548.217d + 18.271f + 1.726N + 3886.848d^2 - 3.566 \times 10^{-1}f^2 - 4.426 \times 10^{-4}N^2 + 108.415df - 1.070dN - 4.848 \times 10^{-2}fN \quad (12)$$

$R^2 = 0.978$

Table 1 Experimental results for core-center drill in drilling carbon fiber composite materials

Test no.	Factor			Thrust force (N)
	Diameter ratio (mm/mm)	Feed rate (mm/min)	Spindle speed (rpm)	
1	0.40	8	800	81.2
2	0.40	8	1,000	65.8
3	0.40	8	1,200	35.8
4	0.40	12	800	125.4
5	0.40	12	1,000	75.1
6	0.40	12	1,200	61.3
7	0.40	16	800	169.7
8	0.40	16	1,000	135.4
9	0.40	16	1,200	75.8
10	0.55	8	800	116.6
11	0.55	8	1,000	103.4
12	0.55	8	1,200	67.1
13	0.55	12	800	208.6
14	0.55	12	1,000	112.6
15	0.55	12	1,200	92.6
16	0.55	16	800	326.6
17	0.55	16	1,000	205.7
18	0.55	16	1,200	98.5
19	0.74	8	800	318.0
20	0.74	8	1,000	295.3
21	0.74	8	1,200	226.6
22	0.74	12	800	583.8
23	0.74	12	1,000	539.8
24	0.74	12	1,200	365.0
25	0.74	16	800	765.4
26	0.74	16	1,000	703.1
27	0.74	16	1,200	435.7

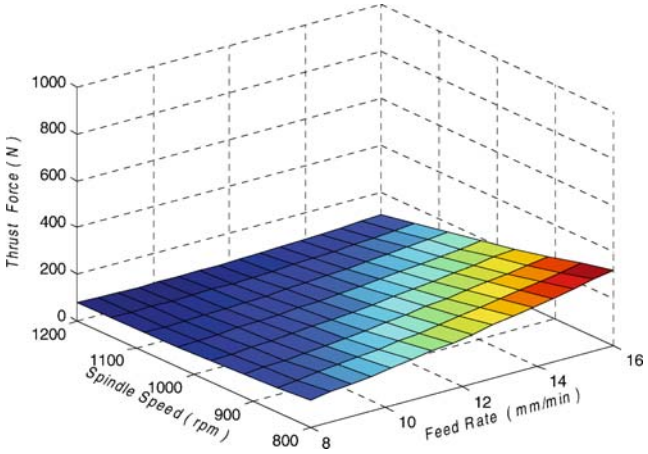

Fig. 4 Response surface plot of thrust force with feed rate and spindle speed (diameter ratio=0.55 mm/mm)

From the developed RSM-based mathematical model, the effect of feed rate and spindle speed on thrust force is shown in Fig. 4. Diameter ratio is taken as constant at 0.55 mm/mm. The thrust force decreases with increasing spindle speed as the feed rate of the drill decreases. As seen in the response plot, the thrust force varies almost linearly with the feed rate. At a high feed rate, a relatively large thrust is obtained while at low feed rate, a small thrust force is observed. The results agree with the industrial practice. Figures 5 and 6 show the different diameters of the inner twist drill, which result not only in different levels of thrust during drilling, but also different values of critical thrust force causing delamination. As seen in the figures, the feed rate and spindle speed are taken as constant at 12 mm/min and 1,000 rpm, respectively. The surface plots in Figs. 5 and 6 reflect that the diameter ratio has a nonlinear effect on thrust force at different feed rates and spindle speeds, respectively. The two figures also show that the thrust force increases with diameter ratio at a faster rate. A greater diameter ratio generates a higher thrust force, which increases delamination. The chips produced by the larger

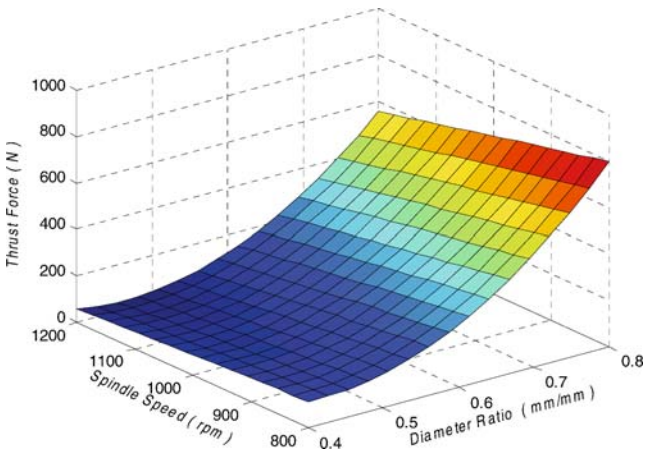

Fig. 5 Response surface plot of thrust force with diameter ratio and spindle speed (feed rate=12 mm/min)

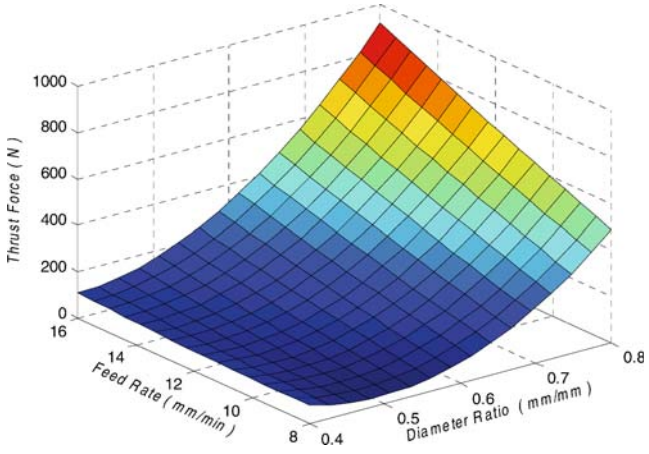

Fig. 6 Response surface plot of thrust force with diameter ratio and feed rate (spindle speed=1,000 rpm)

inner twist drill of core-center drill clink easily with the inner space of core-center drill during drilling. As shown in Fig. 6, the interaction of diameter ratio with feed rate has the most significant effect on the drilling-induced thrust force. However, at a higher spindle speed, the amount of variation in thrust force due to the increase in diameter ratio is comparatively lower. In addition, a higher spindle speed helps remove excess heat rapidly and also eject the chips produced during cutting.

5.2 Analysis of RBFN

The learning process of RBFN is iterative in that the entire training set is presented to the neural network repeatedly until the RMSE reaches an acceptable value. The training data acquired from experimental results were substituted into the RBFN mode, and the epoch number is 5,000. In this paper, the RBFN is good enough to produce a satisfactory result after 350 iterations. In consideration of the precision and computing time, different epoch numbers were compared in this study. After several trial-and-error iterations, the hidden neuron number is set 48, the initial weighting is 0.5, the momentum constant (α) is 0.009, and the learning rate (η) is 0.0021. Once the prediction mode of thrust force is established, the drilling-induced thrust force

Table 2 Drilling conditions in verification tests

Test no.	d (mm/mm)	f (mm/min)	N (rpm)
1	0.40	8.2	800
2	0.40	10.5	920
3	0.40	13.0	1,000
4	0.55	8.8	860
5	0.55	11.5	1,020
6	0.55	14.0	1,200
7	0.74	9.5	820
8	0.74	12.5	1,050
9	0.74	15.5	1,150

Table 3 Experimental results and comparison with RSM model and RBFN

Test no.	Thrust force (N)				
	Experimental values	RSM model of Eq. (12)	ABS. error (%)	RBFN	ABS. error (%)
1	60.5	63.7	5.29	60.5	0
2	96.2	104.3	8.42	96.2	0
3	100.5	111.3	10.75	100.5	0
4	118.4	108.7	8.19	118.1	0.25
5	164.7	146.6	10.99	163.8	0.55
6	112.8	100.7	10.73	112.3	0.44
7	467.1	439.6	5.89	465.9	0.26
8	502.4	477.5	4.96	500.1	0.46
9	557.6	511.2	8.32	555.4	0.39

for various drilling parameters can be predicted in a quick and accurate manner.

5.3 Confirmation test

The drilling conditions used in the confirmation tests are shown in Table 2. Table 3 displays the comparison between the values predicted by the RSM model using Eq. (12) and those obtained by the RBFN developed in this study. As can be seen, the results obtained by the RSM model (Eq. 12) has average absolute deviation of less than 11%, while the average absolute errors of thrust force when using RBFN are below 0.6%. The comparison between the predicted and measured thrust force for RBFN is shown in Fig. 7. Our findings show that the RBFN is more precise than the RSM model (Eq. 12). RBFN is thus demonstrated to be a practical and effective way for the evaluation of drilling-induced thrust force.

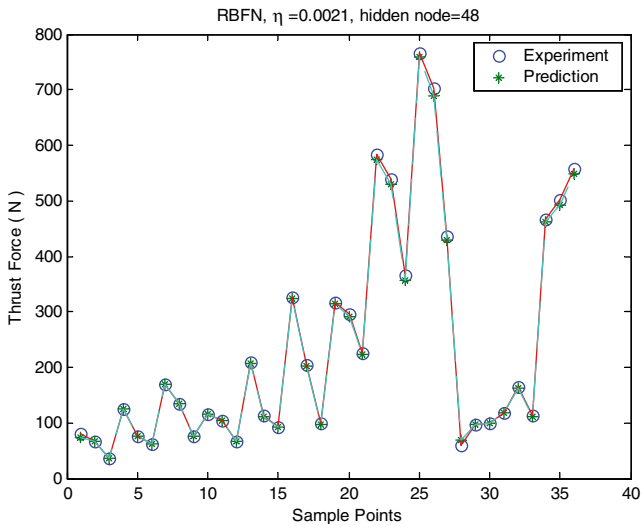

Fig. 7 Comparisons of prediction and experimental thrust force using RBFN

5.4 Comparison of thrust force among twist drill, core drill and core-center drill

According to the push-out model [16, 33, 34], the critical thrust force for various drill bits (twist drill, core drill and core-center drill) are

$$F_A = \pi\left[\frac{8G_{IC}E_M h^3}{3(1-\nu^2)}\right]^{1/2} = \pi\sqrt{32G_{IC}M} \tag{13}$$

$$F_R = \pi\left\{\frac{32G_{IC}M}{1-\left[\left(2-2\beta+\frac{3\beta^2}{2}\right)+\frac{4(1-\beta)^2}{\beta(2-\beta)}\ln(1-\beta)\right]s^2 + \left[\frac{(2-4\beta+5\beta^2-3\beta^3+\beta^4)}{2}+\frac{2(1-\beta)^2(2-2\beta+\beta^2)}{\beta(2-\beta)}\ln(1-\beta)\right]s^4}\right\}^{1/2} \tag{14}$$

$$F_{CC} = \pi(1+\gamma)\left\{\frac{32G_{IC}M}{\gamma^2+\left\{\begin{array}{l}1-\left[\left(2-2\beta+\frac{3\beta^2}{2}\right)+\frac{4(1-\beta)^2}{\beta(2-\beta)}\ln(1-\beta)\right]s^2 \\ +\left[\frac{(2-4\beta+5\beta^2-3\beta^3+\beta^4)}{2}+\frac{2(1-\beta)^2(2-2\beta+\beta^2)}{\beta(2-\beta)}\ln(1-\beta)\right]s^4\end{array}\right\}}\right\}^{1/2} \tag{15}$$

where $M = \frac{E_M h^3}{12(1-\nu^2)}$ is called flexural rigidity of the plate, E_M is the modulus of elasticity, G_{IC} is the energy release rate, h is the uncut depth under tool, ν is the Poisson's ratio, β is the ratio between thickness (t) and outside radius of core drill (c), γ is the ratio of the central concentrated force and the annular area force, s is the ratio of drill radius and delamination radius (namely, $s = c^*/a$).

The core-center drill exerts a thrust force on the laminate, which is composed of the concentrated central force and the annular load. Since the total thrust force is

Table 4 Critical thrust force of twist drill, core drill and core-center drill

Drill bit	Theoretical critical thrust force (N)	Experimental critical thrust force (N)	ABS error (%)
Twist drill [16]	34.1	31.8	6.6
Core drill [16]	48.4	42.7	11.8
Core-center drill	48.6	45.7	6.0

distributed towards the periphery at a ratio of γ (Eq. 15), the drill is expected to have the advantage of allowing a larger critical thrust force at the onset of delamination, similar to the effect of core drill. The larger the γ, the larger the critical thrust force will be. In fact, the core-center drill is physically intermediate between the twist drill and the core drill, and mathematically the general solution is reducible to the particular cases of either twist drill (completely concentrated force) or core drill (completely annular load). The analytical and experimental critical thrust force of twist drill, core drill and core-center drill at onset of drilling-induced delamination are shown in Table 4. As can be seen, core-center drill can offer higher thrust force than twist drill or core drill. It also implies that twist drill is more susceptible to causing delamination damage when drilling at the same feed rate, not to mention that its threshold thrust at the onset of delamination is the lowest among the three. The center portion (twist drill) of the core-center drill can reduce thrust force caused by the chips clogged inside the core drill.

6 Conclusion

When drilling CFRP with a core-center drill, the diameter ratio and feed rate have a very significant effect on the thrust force. Thrust force increases with an increase in the diameter ratio and feed rate and decreases with increase in spindle speed. Thrust force has an increasing curvilinear nature with increase in diameter ratio and feed rate. However, at higher spindle speed, the amount of variation in thrust force due to increase in diameter ratio is comparatively lower. In addition, a higher spindle speed helps remove excess heat rapidly and also ejects the chips produced during cutting. This study also compared the response surface methodology with RBFN techniques in predicting drilling-induced thrust force using various drilling parameters (diameter ratio, feed rate, and spindle speed). It was found that the RBFN is more precise than the RSM model in experimental drilling prediction. However, the prediction by RBFN techniques requires proper setting of parameters, such as number of hidden neurons, momentum constant, and learning rate.

Acknowledgements This work was supported by funding from Tahua Institute of Technology, Taiwan, ROC, under contract TH-93-2-AE-06.

References

1. Ravishankar SR, Murthy CRL (1996) Ultrasonic imaging for evaluation of drill-induced delaminations in composite laminates. In: Proceedings of the 14th World Conference Nondestructive Test, 8–13 December. New Delhi, India, pp 489–494
2. Galloway DF (1957) Some experiments on the influence of various factors on drill performance. ASME 79:191–237
3. Russell WR (1962) Drill design and drilling conditions for improved efficiency. ASTME Paper No. 397 p.62
4. Wu SM, Shen JM (1983) Mathematical model for multifacet drills. ASME J Eng Ind 105:173–182
5. Doerr R, Greene E, Lyon B, Taha S (1982) Development of effective machining and tooling techniques for Kevlar composites. Technical Report, No. AD-A117853
6. Friedrich MO, Burant RO, McGinty MJ (1979) Cutting tools/drills: part 5 - point styles and applications. Manuf Eng 83:29–31
7. Haggerty WA, Ernst H (1958) The spiral point drill - self-centering drill point geometry. ASTE Paper No. 101 p.58
8. Koenig W, Wulf C, Grass P, Willerscheid H (1985) Machining of fiber reinforced plastics. Ann CIRP 34(2):538–548
9. Tagliaferri V, Caprino G, Diterlizzi A (1990) Effect of drilling parameters on the finish and mechanical properties of GFRP composites. Inter J Mach Tools Manuf 30(1):77–84
10. Davim JP, Reis P (2003) Study of delamination in drilling carbon fiber reinforced plastics (CFRP) using design experiments. Compos Struct 59(4):481–487
11. Tsao CC, Hocheng H (2004) Taguchi analysis of delamination associated with various drill bits in drilling of composite material. Int J Mach Tools Manuf 44(10):1085–1090
12. Komanduri R (1993) Machining fiber-reinforced plastics. ASME Mech Eng 115(4):58–64
13. Davidson BD, Altonen CS, Polaha JJ (1996) Effect of stacking sequence on delamination toughness and delamination growth behavior in composite end-notched flexure specimens. ASTM Spec Tech Publ 1274:393–413
14. Jung JP, Kim GW, Lee KY (2005) Critical thrust force at delamination propagation during drilling of angle-ply laminates. Compos Struct 68(4):391–397
15. Hocheng H, Tsao CC (2003) Comprehensive analysis of delamination in drilling of composite materials with various drill bits. J Mater Process Technol 140:335–339
16. Hocheng H, Tsao CC (2006) Effects of special drill bits on drilling-induced delamination of composite materials. Inter J Mach Tools Manuf 46:1403–1416
17. Mathew J, Ramakrishnan N, Naik NK (1999) Investigations into the effect of geometry of a trepanning tool on thrust and torque during drilling of GFRP composites. J Mater Process Technol 91:1–11
18. Piquet R, Ferret B, Lachaud F, Swider P (2000) Experimental analysis of drilling damage in thin carbon/epoxy plate using special drills. Compos Part A: Appl Sci Manuf 31(10):1107–1115
19. Kuar AS, Doloi B, Bhattacharyya B (2006) Modelling and analysis of pulsed Nd:YAG laser machining characteristics during

micro-drilling of zirconia (ZrO2). Inter J Mach Tools Manuf 46:1301–1310
20. Onwubolu GC, Kumar S (2006) Response surface methodology-based approach to CNC drilling operations. J Mater Process Technol 171:41–47
21. Chiang KT, Chang FP, Tsai DC (2007) Modeling and analysis of the rapidly resolidified layer of SG cast iron in the EDM process through the response surface methodology. J Mater Process Technol 182:525–533
22. Özel T, Karpat Y (2005) Predictive modeling of surface roughness and tool wear in hard turning using regression and neural networks. Inter J Mach Tools Manuf 45:467–479
23. Panda SS, Singh AK, Chakraborty D, Pal SK (2006) Drill wear monitoring using back propagation neural network. J Mater Process Technol 172(2):283–290
24. Tsai KM, Wang PJ (2001) Predictions on surface finish in electrical discharge machining based upon neural network models. Inter J Mach Tools Manuf 41(10):1385–1403
25. Tsao CC (2002) Prediction of flank wear of different coated drills for JIS SUS 304 stainless steel using neural network. J Mater Process Technol 123(3):354–360
26. Chen WC, Hsu SW (2007) A neural-network approach for an automatic LED inspection system. Expert Sys Appl 33(2): 531–537
27. Jang JSR, Sun CT (1993) Functional equivalence between radial basis function networks and fuzzy inference systems. IEEE Trans Neural Networks 4(1):156–159
28. Mason JD, Craddock RJ, Mason JC, Parks PC, Warwick K (1994) Towards a stability and approximation theory for neuro-controllers. In: Proceedings of the International Conference on Control 94, 21–24 March, Coventry, UK, 1: pp. 100–103
29. Kim B, Park K (2005) Modeling plasma etching process using a radial basis function network. Microelectron Eng 77(2):150–157
30. Zhang Z, Friedrich K (2003) Artificial neural networks applied to polymer composites: a review. Compos Sci Technol 63(14):2029–2044
31. Box GEP, Draper NR (1987) Empirical model-building and response surface. Wiley, New York
32. Haykin S (1999) Neural networks: a comprehensive foundation. Prentice Hall, Upper Saddle River, NJ
33. Hocheng H, Dharan CKH (1990) Delamination during drilling in composite laminates. ASME J Eng Ind 112:236–239
34. Hocheng H, Tsao CC (2005) The path towards delamination-free drilling of composite materials. J Mater Process Technol 167:251–264